Hindawi
Journal of Sensors
Volume 2018, Article ID 1738014, 12 pages
https://doi.org/10.1155/2018/1738014

Research Article

Ocean Wave Information Retrieval Using Simulated Compact Polarized SAR from Radarsat-2

Xiaochen Wang[1,2,3] **Yun Shao**[1,2,3,4] **Lu She**[2,3] **Wei Tian**[1,2,3] **Kun Li**[1,2,3] **and Long Liu**[1,2,3]

[1]*Laboratory of Target Microwave Properties, Deqing Academy of Satellite Applications, Huzhou 313200, China*
[2]*Institute of Remote Sensing and Digital Earth, Chinese Academy of Sciences, 1 Beichen Road, Beijing 100101, China*
[3]*University of Chinese Academy of Sciences, 19A Yuquan Road, Beijing 100049, China*
[4]*State Key Laboratory of Remote Sensing Science, Institute of Remote Sensing and Digital Earth, Chinese Academy of Sciences, 1 Beichen Road, Beijing 100101, China*

Correspondence should be addressed to Lu She; shelu_whu@163.com

Received 17 October 2017; Accepted 28 March 2018; Published 7 June 2018

Academic Editor: Biswajeet Pradhan

The main objective of this paper is to demonstrate the capability of compact polarized (CP) synthetic aperture radar (SAR) to retrieve ocean wave field parameters. Souyris' and Nord's algorithms are used to carry out the reconstruction of CP SAR pseudo quad-polarized data for the ocean surface under both the circular transmit linear receive (CTLR) and $\pi/4$ mode. The results show that, for the CP reconstruction, Nord's algorithm has a better convergence ability than Souyris'. In addition, the investigation of the reconstruction accuracy shows that the CTLR mode is superior to the $\pi/4$ mode, in terms of ocean surface reconstruction. It is, therefore, concluded that the reconstructed parameters of CP CTLR mode data by Nord's algorithm adapt to retrieve ocean wave information. The ocean wave slope spectrum and other main wave parameters are also calculated from reconstructed CP data and compared with measurements from in situ National Data Buoy Center (NDBC) matched-up buoys. Comparison of CP SAR-based wave field information with buoy outputs also shows good agreement in the case of dominate wave height, wave direction, and wave period, with biases of 0.36 m, 17.96°, and 0.88 s, respectively.

1. Introduction

Ocean waves are the most important ocean surface features in the fields of ocean physics and coastal engineering. Ocean surface parameters, such as wave height, wave direction, and wave length, are important for sea-ice monitoring, ship detection, marine pollution forecasting, and in other areas [1, 2]. The wave slope spectrum, which provides information about the 2-D directional distribution of the wave energy density, is important to ocean wave information retrieval. In recent years, remote sensing as an efficient tool for earth surface monitoring gradually plays a key role in ocean information retrieval. Of all remote sensing sensors, SAR systems are the active satellite sensors with a resolution high enough to provide information about the ocean wave spectrum and so these systems play a key role in the measurement of ocean surface waves [3–5]. In contrast to in situ buoys, SAR can operate in all weather conditions or in areas far from the shore and can measure ocean waves across the globe continuously [6]. In addition to improving the understanding of the properties of the ocean, SAR observations can be used to develop the forecast accuracy of the operational wave model. It is, therefore, important to investigate the capability of SAR to carry out ocean surface monitoring, especially in terms of ocean wave retrieval.

In recent decades, satellites such as ERS-1, ERS-2, Envisat, Radarsat-1/2, Sentinel-1 A/B, and Chinese GF-3 have carried on many SAR systems for use in ocean surface monitoring. Several wave retrieval algorithms have also been developed for ocean information retrieval. For example, K.

Hasselmann and S. Hasselmann [7, 8] proposed the Max Planck Institute (MPI) algorithm based on the closed nonlinear transformation relation between the ocean spectrum and the SAR image spectrum; the output from the wave model (WAM) is input as a first-guess spectrum in this method. Mastenbroek and de Valk [9] developed a semiparametric retrieval algorithm (SPRA) based on Hasselmann's nonlinear theory [7] by separating the wind-driven wave and swell—the wind-wave information is provided by synchronous scatterometer measurements and the swell information is derived from the rest of the SAR signal. Wang [10] proposed a semiempirical algorithm which has the objective to estimate the wave height from Envisat ASAR wave mode imagery without any prior knowledge. Shao et al. [11] develop a semiempirical function for significant wave height (Hs) and mean wave period (Tmw) retrieval from C-band VV polarization Sentinel-1 SAR. With the development of polarization technology, quad-polarized SAR has also been applied in ocean surface monitoring. Zhang et al. [12] present a synergistic method to retrieve both ocean surface wave and wind fields from spaceborne quad-polarization SAR, with consideration to the nonlinear mapping relationship between ocean wave spectra and SAR image spectra, in order to synergistically retrieve wind fields and wave directional spectra. Schuler and Lee [13, 14] proposed an algorithm for retrieving ocean wave spectra using quad-polarized SAR imagery and also investigated the results using L- and P-band SAR data. However, this method is only suitable for the L and P bands. By modifying the polarization orientation angle, He et al. [15, 16] developed a new retrieval algorithm so that it could be applied to C-band quad-polarized SAR data. He et al.'s method was also validated using Radarsat-2 quad-polarized SAR data by Zhang et al. [17, 18].

In addition, although the quad-polarized SAR can provide abundant polarization information to develop the process of ocean information retrieval, the limited swath width has also become the disadvantage of quad-polarized SAR for large-scale monitoring. For overcoming the limitation of CP SAR, a new type of SAR sensor called compact p(CP) SAR has been invented, which provides a new way to measure ocean waves and its potential for use in ocean surface monitoring has gradually become clear [19]. Compared with quad-polarized SAR, CP SAR operates at lower power but still has the capability to reconstruct quad-polarized data, thus overcoming the disadvantages of the narrow swath and high power of quad-polarized SAR and the insufficient polarized information provided by single- or dual-polarized SAR [20, 21]. CP SAR can, in fact, be interpreted as a compromise between dual-polarized and quad-polarized SAR so that swath width is increased and the operating power is reduced at the same time. To date, India's RISAT-1, launched in April 2012, and the Japanese ALOS-2 SAR satellite, launched in May 2014, have carried CP SAR. In the future, the planned Radarsat-2 constellation of satellites will also support CP SAR. Although CP SAR is carried on existing SAR platforms, there is still no well-calibrated data that can be used in research, especially in the case of ocean wave measurements. It is, therefore, important to study the potential of CP SAR for the retrieval of ocean wave information. In a previous study, Nunziata et al. [22] investigated sea-surface scattering with a polarized model and exploited the hybrid polarized (HP) mode to interpret ocean surface polarization parameters. Yin et al. [23] proposed a new extended X-Bragg model and also used C-band quad-polarized SAR data acquired by both SIR-C/X-SAR and Radarsat-2 to emulate the HP and $\pi/4$ CP modes. Geldsetzer et al. [24] proposed that the dependence between incidence angle, wind speed, and wind direction of CP SAR parameters are presented for open water. Selected 20 CP parameters are related to C-band geophysical model function (CMOD) output. CP parameters are simulated from polarized Radarsat-2 data and emulate data available on the pending Radarsat Constellation Mission (RCM). Li et al. [25] present a new empirical reconstruction algorithm for the modified N based on a data set of more than 2000 Radarsat-2 quad-polarization images and collocated buoy observations. It is proven that cross-polarization facilitates wind speed retrieval and improves the accuracy of the results, especially with respect to high wind speeds. In summary, the capability of CP SAR to reconstruct pseudo quad-pol data and ocean wind retrieval has been investigated in detailed; however, its potential for ocean surface reconstruction has not been discussed yet, let alone wave information retrieval.

In this paper, two quad-polarized SAR images are used to reconstruct the CP pseudo quad-polarized data and demonstrate the potential of CP SAR for ocean wave information retrieval. The data set used in this paper is illustrated in Section 2. In Section 3, we briefly introduced the CP theory and the ocean wave retrieval method. In Section 4, we investigate two CP algorithms used for ocean surface reconstruction and evaluate the optimum CP mode for ocean surface reconstruction. The FP and CP ocean wave retrieval results are compared with NDBC buoy data. Conclusions are given in Section 5.

2. Data Sets

2.1. SAR Data. Two scenes of Radarsat-2 quad-polarized image are used in this study. Both of two image acquisition parameters are listed in Table 1, and the study areas are shown in Figures 1(a) and 1(b). HH-, HV-, and VV-polarized single look complex image (SLC) SAR images are also shown in Figures 1(a) and 1(b).

2.2. Buoy Data. In order to validate the CP SAR wave retrieval results, NDBC buoy data available from the National Oceanic and Atmospheric Administration (NOAA) were collected along with the SAR imagery. The main wave parameters were extracted from the original measurements and are listed in Table 2. Among all the wave measurement data, the dominant wave height (DWH), the dominant wave period (DWP), and dominant wave direction (DWD) were used for validating the retrieval results.

Because of limited collection of NDBC buoy, only one buoy was collocated with SAR imagery of scene 2. So the imagery of scene 1 was performed to CP reconstruction and ocean slope spectrum retrieval methods, and scene 2 was added to validate the method.

Table 1: Radar parameters of C-band Radarsat-2 quad-polarized data used for this study.

Scene ID	Image file name	Observation time	Incidence angle	Scene position	
				Latitude	Longitude
1	RS2-SLC-FQ3-ASC-31-Mar-2008_18.10-PDS_00058910	31 Mar. 2008 18:10	20.8°–22.8°	35.96°N	5.65°W
2	RS2-SLC-FQ9-ASC-09-Apr-2008_02.01-PDS_00058900	09 Apr. 2008 02:01	28.0°–29.8°	37.82°N	122.46°W

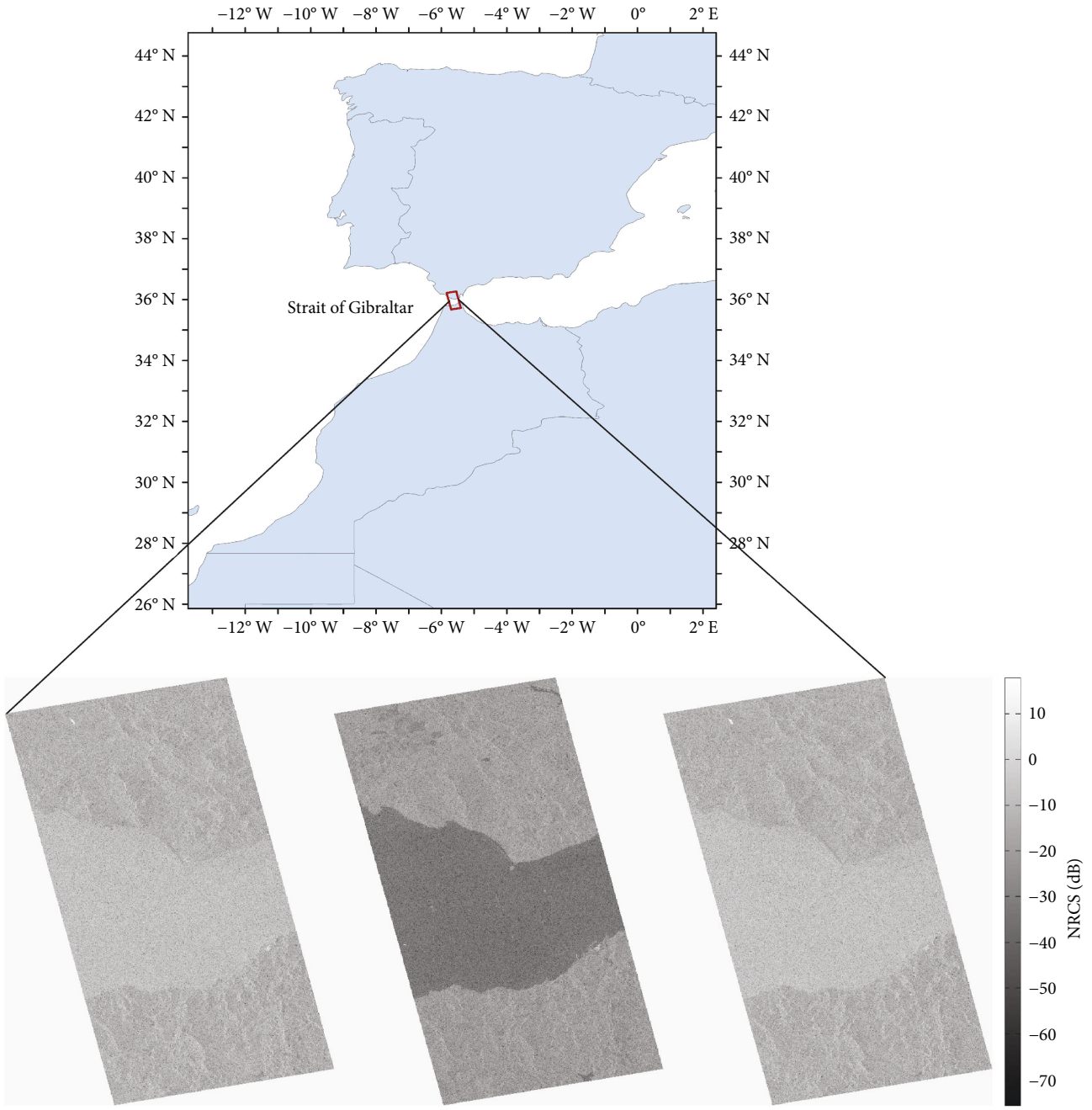

(A) HH (B) HV (VH) (C) VV

(a)

Figure 1: Continued.

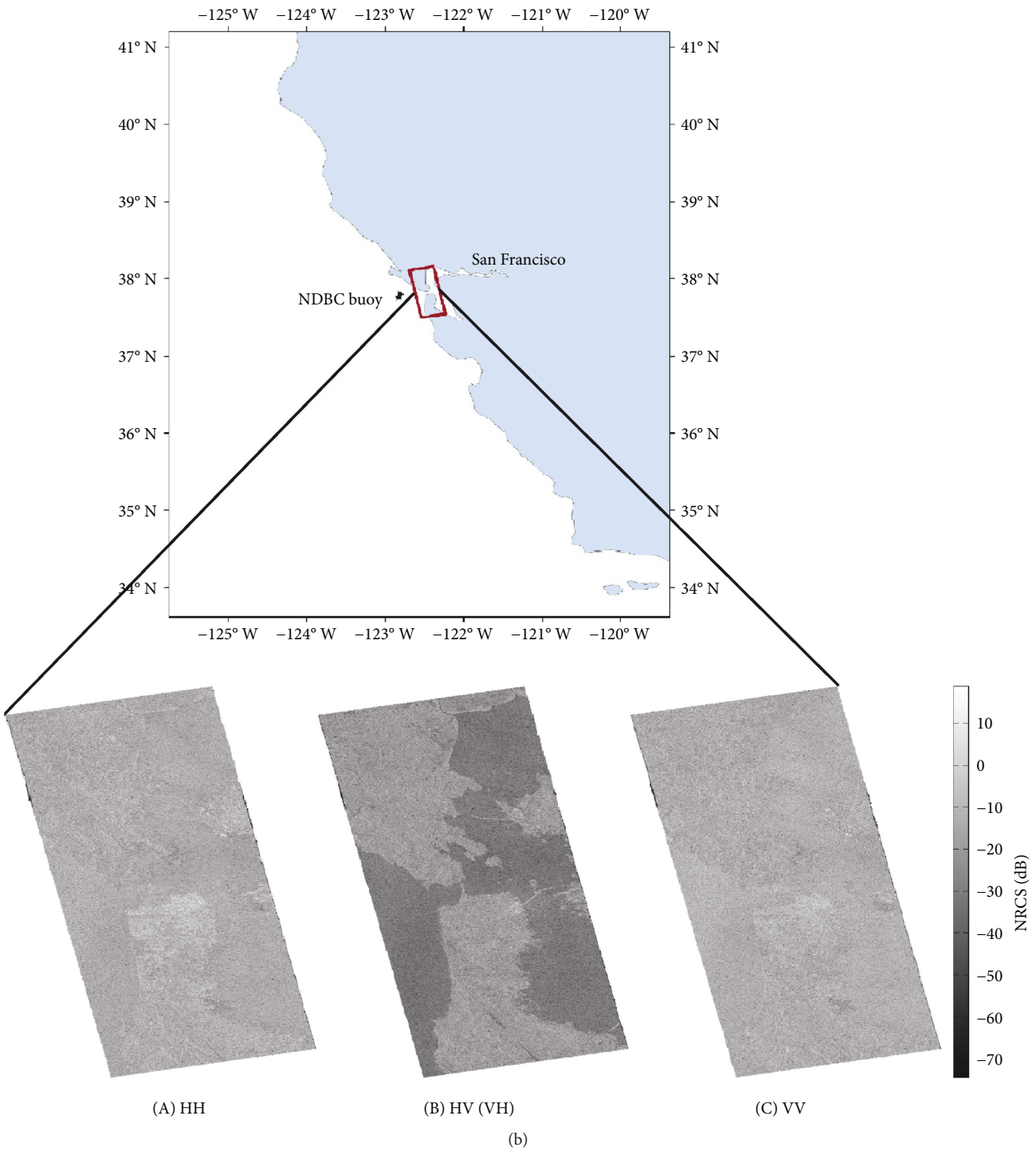

Figure 1: (a) The study area of scene 1: the coast near Strait of Gibraltar. The Radarsat-2 quad-polarized SLC SAR image was acquired on 2008/4/1. (A–C) correspond to the HH, HV (VH), and VV polarization channels, respectively. (b) The study area of scene 2: the coast near San Francisco. The Radarsat-2 quad-polarized SLC SAR image was acquired on 2008/4/9. The radar image and NDBC buoys are also marked. (A–C) correspond to the HH, HV (VH), and VV polarization channels, respectively.

3. Theory and Method

3.1. CP Reconstruction. CP theory is a newly developed method that can produce pseudo quad-polarized data from dual-polarized SAR data. The polarized information can be reconstructed in a satisfied precision with the decrease of sensor operation power [26, 27]. The CP has three main modes: the CTLR, dual circular polarized (DCP), and $\pi/4$ modes.

3.1.1. CTLR Mode. In the CTLR mode, the microwaves are transmitted in left-handed or right-handed circular

Table 2: Standard meteorological record from an NDBC in situ buoy.

Buoy ID	46237
Date	2008/4/9 01:51
Location	37.786 N 122.634 W
Water depth (m)	16.8
Dominant wave height (m)	2.18
Dominant wave period (s)	14.29
Average wave period (s)	7.03
Mean wave direction (°)	246

polarization and received in HH and VV polarization. The scattering vector $\vec{\mathbf{k}}_{\mathrm{CTLR}}$ is expressed as

$$\vec{\mathbf{k}}_{\mathrm{CTLR}} = \frac{[S_{\mathrm{hh}} - iS_{\mathrm{hv}} - iS_{\mathrm{vv}} + S_{\mathrm{hv}}]^T}{2}. \tag{1}$$

The relevant Hermitian covariance matrix is

$$\begin{aligned}\mathbf{C}_{\mathrm{CTLR}} &= \left\langle \vec{\mathbf{k}}_{\mathrm{CTLR}} \vec{\mathbf{k}}^{*T}_{\mathrm{CTLR}} \right\rangle \\ &= \frac{1}{2}\begin{bmatrix} \langle |\mathbf{S}_{\mathrm{hh}}|^2 \rangle & \langle i(\mathbf{S}_{\mathrm{hh}}\mathbf{S}^*_{\mathrm{vv}}) \rangle \\ \langle -i(\mathbf{S}_{\mathrm{vv}}\mathbf{S}^*_{\mathrm{hh}}) \rangle & \langle |\mathbf{S}_{\mathrm{vv}}|^2 \rangle \end{bmatrix} \\ &\quad + \frac{1}{2}\langle |\mathbf{S}_{\mathrm{hv}}|^2 \rangle \begin{bmatrix} 1 & -i \\ i & 1 \end{bmatrix} \\ &\quad + \frac{1}{2}\begin{bmatrix} -2\Im(\langle \mathbf{S}_{\mathrm{hh}}\mathbf{S}^*_{\mathrm{hv}} \rangle) & \langle \mathbf{S}_{\mathrm{hh}}\mathbf{S}^*_{\mathrm{hv}} \rangle + \langle \mathbf{S}_{\mathrm{hv}}\mathbf{S}^*_{\mathrm{vv}} \rangle \\ \langle \mathbf{S}^*_{\mathrm{hh}}\mathbf{S}_{\mathrm{hv}} \rangle + \langle \mathbf{S}_{\mathrm{vv}}\mathbf{S}^*_{\mathrm{hv}} \rangle & 2\Im(\langle \mathbf{S}_{\mathrm{vv}}\mathbf{S}^*_{\mathrm{hv}} \rangle) \end{bmatrix}, \end{aligned} \tag{2}$$

where T stands for matrix transpose operations, $*$ stands for matrix conjugate operations, $\langle\rangle$ stands for average operations, $\Re$ is the real part of complex number, $\mathbf{S}_{\mathrm{pq}}$ is polarization scattering matrix and p, q are horizontal or vertical polarized channel, i is the imaginary unit, and $\Im$ is the imaginary part of complex number. It is also noticeable that this matrix can be simplified based on the assumption that the reflection is symmetrical.

$$\begin{aligned}\mathbf{C}_{\mathrm{CTLR}} &= \left\langle \vec{\mathbf{k}}_{\mathrm{CTLR}} \vec{\mathbf{k}}^{*T}_{\mathrm{CTLR}} \right\rangle \\ &= \frac{1}{2}\begin{bmatrix} \langle |\mathbf{S}_{\mathrm{hh}}|^2 \rangle & \langle i(\mathbf{S}_{\mathrm{hh}}\mathbf{S}^*_{\mathrm{vv}}) \rangle \\ \langle -i(\mathbf{S}_{\mathrm{vv}}\mathbf{S}^*_{\mathrm{hh}}) \rangle & \langle |\mathbf{S}_{\mathrm{vv}}|^2 \rangle \end{bmatrix} \\ &\quad + \frac{1}{2}\langle |\mathbf{S}_{\mathrm{hv}}|^2 \rangle \begin{bmatrix} 1 & -i \\ i & 1 \end{bmatrix}. \end{aligned} \tag{3}$$

In order to reconstruct a pseudo quad-polarized covariance matrix for the CP CTLR mode, $\langle |\mathbf{S}_{\mathrm{hv}}|^2 \rangle$ also needs to be iteratively solved. This covariance matrix can be expressed as

$$\begin{aligned}&[\mathbf{C}_{\mathrm{CTLR}}]_{\mathrm{pseudo-quad}} \\ &= \begin{bmatrix} C_{11} - \langle |\mathbf{S}_{\mathrm{hv}}|^2 \rangle & 0 & iC_{12} + \langle |\mathbf{S}_{\mathrm{hv}}|^2 \rangle \\ 0 & 2\langle |\mathbf{S}_{\mathrm{hv}}|^2 \rangle & 0 \\ (iC_{12} + \langle |\mathbf{S}_{\mathrm{hv}}|^2 \rangle)^* & 0 & C_{22} - \langle |\mathbf{S}_{\mathrm{hv}}|^2 \rangle \end{bmatrix}. \end{aligned} \tag{4}$$

It is noticed that C_{ij} in (4) is element from CP 2×2 covariance matrix.

3.1.2. DCP Mode. In DCP mode, the microwaves are transmitted in right-handed circular polarization and received in left-handed or right-handed circular polarization. The scattering vector $\vec{\mathbf{k}}_{\mathrm{DCP}}$ is expressed as

$$\vec{\mathbf{k}}_{\mathrm{DCP}} = \frac{[\mathbf{S}_{\mathrm{hh}} - \mathbf{S}_{\mathrm{vv}} + i2\mathbf{S}_{\mathrm{hv}}\ i(\mathbf{S}_{\mathrm{hh}} + \mathbf{S}_{\mathrm{vv}})]^T}{2}. \tag{5}$$

The relevant Hermitian covariance matrix is

$$\begin{aligned}\mathbf{C}_{\mathrm{DCP}} &= \left\langle \vec{\mathbf{k}}_{\mathrm{DCP}} \vec{\mathbf{k}}^{*T}_{\mathrm{DCP}} \right\rangle \\ &= \frac{1}{4}\begin{bmatrix} \langle |\mathbf{S}_{\mathrm{hh}} - \mathbf{S}_{\mathrm{vv}}|^2 \rangle & \langle -i(\mathbf{S}_{\mathrm{hh}} - \mathbf{S}_{\mathrm{vv}})(\mathbf{S}_{\mathrm{hh}} + \mathbf{S}_{\mathrm{vv}})^* \rangle \\ \langle -i(\mathbf{S}_{\mathrm{hh}} + \mathbf{S}_{\mathrm{vv}})(\mathbf{S}_{\mathrm{hh}} - \mathbf{S}_{\mathrm{vv}})^* \rangle & \langle |\mathbf{S}_{\mathrm{hh}} + \mathbf{S}_{\mathrm{vv}}|^2 \rangle \end{bmatrix} \\ &\quad + \frac{1}{4}\begin{bmatrix} 4\langle |\mathbf{S}_{\mathrm{hv}}|^2 \rangle & 0 \\ 0 & 0 \end{bmatrix} \\ &\quad + \frac{1}{4}\begin{bmatrix} 4\Im(\langle (\mathbf{S}_{\mathrm{hh}} - \mathbf{S}_{\mathrm{vv}}) \cdot \mathbf{S}^*_{\mathrm{hv}} \rangle) & 2\langle (\mathbf{S}_{\mathrm{hh}} + \mathbf{S}_{\mathrm{vv}})^* \rangle \\ 2\langle (\mathbf{S}_{\mathrm{hh}} + \mathbf{S}_{\mathrm{vv}}) \cdot \mathbf{S}^*_{\mathrm{hv}} \rangle & 0 \end{bmatrix}. \end{aligned} \tag{6}$$

It should be noted that the last term can be set to zero based on the assumption of reflectional symmetry and that the covariance matrix can be simplified to

$$\begin{aligned}\mathbf{C}_{\mathrm{DCP}} &= \left\langle \vec{\mathbf{k}}_{\mathrm{DCP}} \vec{\mathbf{k}}^{*T}_{\mathrm{DCP}} \right\rangle \\ &= \frac{1}{4}\begin{bmatrix} \langle |\mathbf{S}_{\mathrm{hh}} - \mathbf{S}_{\mathrm{vv}}|^2 \rangle & \langle -i(\mathbf{S}_{\mathrm{hh}} - \mathbf{S}_{\mathrm{vv}})(\mathbf{S}_{\mathrm{hh}} + \mathbf{S}_{\mathrm{vv}})^* \rangle \\ \langle -i(\mathbf{S}_{\mathrm{hh}} + \mathbf{S}_{\mathrm{vv}})(\mathbf{S}_{\mathrm{hh}} - \mathbf{S}_{\mathrm{vv}})^* \rangle & \langle |\mathbf{S}_{\mathrm{hh}} + \mathbf{S}_{\mathrm{vv}}|^2 \rangle \end{bmatrix} \\ &\quad + \frac{1}{4}\begin{bmatrix} 4\langle |\mathbf{S}_{\mathrm{hv}}|^2 \rangle & 0 \\ 0 & 0 \end{bmatrix}. \end{aligned} \tag{7}$$

In order to reconstruct a pseudo quad-polarized covariance matrix for the CP DCP mode, $\langle |\mathbf{S}_{\mathrm{hv}}|^2 \rangle$ needs to be iteratively solved. This covariance matrix can be expressed as [28]

$$[\mathbf{C}_{\mathrm{DCP}}]_{\mathrm{pseudo-quad}} = \begin{bmatrix} C_{11} - \langle|\mathbf{S}_{\mathrm{hv}}|^2\rangle & 0 & C_{12} + \langle|\mathbf{S}_{\mathrm{hv}}|^2\rangle \\ 0 & 2\langle|\mathbf{S}_{\mathrm{hv}}|^2\rangle & 0 \\ \left(C_{12} + \langle|\mathbf{S}_{\mathrm{hv}}|^2\rangle\right)^* & 0 & C_{22} - \langle|\mathbf{S}_{\mathrm{hv}}|^2\rangle \end{bmatrix}. \tag{8}$$

It is noticed that C_{ij} in (8) is element from CP 2×2 covariance matrix.

3.1.3. $\pi/4$ Mode. In $\pi/4$ mode, the microwaves are transmitted in linear polarization with a 45° inclination and received in HH and VV polarization. The scattering vector $\overrightarrow{\mathbf{k}}_{\pi/4}$ is expressed as

$$\overrightarrow{\mathbf{k}}_{\pi/4} = \frac{[\mathbf{S}_{\mathrm{hh}} + \mathbf{S}_{\mathrm{hv}}\ \mathbf{S}_{\mathrm{vv}} + \mathbf{S}_{\mathrm{hv}}]^T}{\sqrt{2}}. \tag{9}$$

The relevant Hermitian covariance matrix is

$$\begin{aligned}\mathbf{C}_{\pi/4} &= \left\langle \overrightarrow{\mathbf{k}}_{\pi/4} \overrightarrow{\mathbf{k}}^{*T}_{\pi/4} \right\rangle \\ &= \frac{1}{2}\begin{bmatrix} \langle|\mathbf{S}_{\mathrm{hh}}|^2\rangle & \langle\mathbf{S}_{\mathrm{hh}}\mathbf{S}^*_{\mathrm{vv}}\rangle \\ \langle\mathbf{S}_{\mathrm{vv}}\mathbf{S}^*_{\mathrm{hh}}\rangle & \langle|\mathbf{S}_{\mathrm{vv}}|^2\rangle \end{bmatrix} + \frac{1}{2}\langle|\mathbf{S}_{\mathrm{hv}}|^2\rangle\begin{bmatrix} 1 & 1 \\ 1 & 1 \end{bmatrix} \\ &\quad + \frac{1}{2}\begin{bmatrix} 2\mathscr{R}(\langle\mathbf{S}_{\mathrm{hh}}\mathbf{S}^*_{\mathrm{hv}}\rangle) & \langle\mathbf{S}_{\mathrm{hh}}\mathbf{S}^*_{\mathrm{hv}}\rangle + \langle\mathbf{S}_{\mathrm{hv}}\mathbf{S}^*_{\mathrm{vv}}\rangle \\ \langle\mathbf{S}^*_{\mathrm{hh}}\mathbf{S}_{\mathrm{hv}}\rangle + \langle\mathbf{S}_{\mathrm{vv}}\mathbf{S}^*_{\mathrm{hv}}\rangle & 2\mathscr{R}(\langle\mathbf{S}_{\mathrm{vv}}\mathbf{S}^*_{\mathrm{hv}}\rangle) \end{bmatrix}.\end{aligned} \tag{10}$$

It should be noted that the last term can be set to zero based on the assumption of reflectional symmetry and that the covariance matrix can be simplified to

$$\begin{aligned}\mathbf{C}_{\pi/4} &= \left\langle \overrightarrow{\mathbf{k}}_{\pi/4} \overrightarrow{\mathbf{k}}^{*T}_{\pi/4} \right\rangle = \frac{1}{2}\begin{bmatrix} \langle|\mathbf{S}_{\mathrm{hh}}|^2\rangle & \langle\mathbf{S}_{\mathrm{hh}}\mathbf{S}^*_{\mathrm{vv}}\rangle \\ \langle\mathbf{S}_{\mathrm{vv}}\mathbf{S}^*_{\mathrm{hh}}\rangle & \langle|\mathbf{S}_{\mathrm{vv}}|^2\rangle \end{bmatrix} \\ &\quad + \frac{1}{2}\langle|\mathbf{S}_{\mathrm{hv}}|^2\rangle\begin{bmatrix} 1 & 1 \\ 1 & 1 \end{bmatrix}.\end{aligned} \tag{11}$$

In order to reconstruct the pseudo quad-polarized covariance matrix for the CP $\pi/4$ mode, $\langle|\mathbf{S}_{\mathrm{hv}}|^2\rangle$ needs to be iteratively solved. The pseudo quad-polarized covariance matrix for the $\pi/4$ mode can be expressed as [28]

$$[\mathbf{C}_{\pi/4}]_{\mathrm{pseudo-quad}} = \begin{bmatrix} C_{11} - \langle|\mathbf{S}_{\mathrm{hv}}|^2\rangle & 0 & C_{12} - \langle|\mathbf{S}_{\mathrm{hv}}|^2\rangle \\ 0 & 2\langle|\mathbf{S}_{\mathrm{hv}}|^2\rangle & 0 \\ \left(C_{12} - \langle|\mathbf{S}_{\mathrm{hv}}|^2\rangle\right)^* & 0 & C_{22} - \langle|\mathbf{S}_{\mathrm{hv}}|^2\rangle \end{bmatrix}. \tag{12}$$

It is noticed that C_{ij} in (12) is element from CP 2×2 covariance matrix.

It should also be noted that the scattering vectors $\overrightarrow{\mathbf{k}}_{\mathrm{CTLR}}$ and $\overrightarrow{\mathbf{k}}_{\mathrm{DCP}}$ are related by

$$\overrightarrow{\mathbf{k}}_{\mathrm{DCP}} = \frac{1}{\sqrt{2}}\begin{bmatrix} 1 & -i \\ 1 & i \end{bmatrix}\overrightarrow{\mathbf{k}}_{\mathrm{CTLR}}. \tag{13}$$

The polarization information for the CTLR and DCP modes will be similar because of the above linear relationship, which means that the CP reconstruction result for these two modes will be the same [29, 30].

3.2. Wave Spectrum Retrieval Algorithm. For the linearly polarized backscattering cross section, the quad-polarized covariance matrix is used for the ocean surface wave polarization signatures, as follows [31]:

$$\begin{aligned}\mathbf{C} &= \begin{bmatrix} C_{11} & C_{12} & C_{13} \\ C_{21} & C_{22} & C_{23} \\ C_{31} & C_{32} & C_{33} \end{bmatrix} \\ &= \begin{bmatrix} |\mathbf{S}_{\mathrm{hh}}|^2 & \sqrt{2}(\mathbf{S}_{\mathrm{hh}}\mathbf{S}^*_{\mathrm{hv}}) & \mathbf{S}_{\mathrm{hh}}\mathbf{S}^*_{\mathrm{vv}} \\ \sqrt{2}(\mathbf{S}_{\mathrm{hv}}\mathbf{S}^*_{\mathrm{hh}}) & 2|\mathbf{S}_{\mathrm{hv}}|^2 & \sqrt{2}(\mathbf{S}_{\mathrm{hv}}\mathbf{S}^*_{\mathrm{vv}}) \\ \mathbf{S}_{\mathrm{vv}}\mathbf{S}^*_{\mathrm{hh}} & \sqrt{2}(\mathbf{S}_{\mathrm{vv}}\mathbf{S}^*_{\mathrm{hv}}) & |\mathbf{S}_{\mathrm{vv}}|^2 \end{bmatrix}.\end{aligned} \tag{14}$$

It is noticed that C_{ij} in (14) is element from FP 3×3 covariance matrix. Because the maximum contribution to the wave slope is obtained using only linear polarization, here, we set the ellipticity to zero and so the linearly polarized backscattering cross section at any polarization orientation angle can be derived as [14, 15]:

$$\begin{aligned}\sigma(0,\varphi) &= \frac{1}{4}(\sigma_{\mathrm{hh}} + \sigma_{\mathrm{vv}})\left[1 + \cos^2(2\varphi)\right] \\ &\quad + \frac{1}{2}(\sigma_{\mathrm{hh}} - \sigma_{\mathrm{vv}})\cos 2\varphi + \sigma_{\mathrm{hv}} \\ &\quad + \frac{1}{2}\Re(\sigma_{\mathrm{hhvv}})\sin^2(2\varphi),\end{aligned} \tag{15}$$

where σ_{hh}, σ_{hv}, and σ_{vv} are the linearly polarized backscattering cross sections for the horizontal, cross, and vertical polarizations, respectively. σ_{hhvv} is the correlation between the horizontal and vertical polarizations, which can be directly derived from the covariance matrix.

In the linear modulation theory of ocean waves, the ocean surface height can be regarded as a superposition of sine waves and the radar backscattering cross section expressed as [16, 32, 33]

$$\xi(r,t) = \sum_k \xi_k \exp\left[i(k\cdot\mathbf{r} - \omega t)\right] + \mathrm{cc}, \tag{16}$$

$$\sigma_{\mathrm{pp}}(r,t) = \overline{\sigma_{\mathrm{pp}}}\left(1 + \left\{\sum_k T^{\mathrm{R}}_{\mathrm{PPK}}\xi_k \exp\left[i(k\cdot\mathbf{r} - \omega t)\right] + \mathrm{cc}\right\}\right), \tag{17}$$

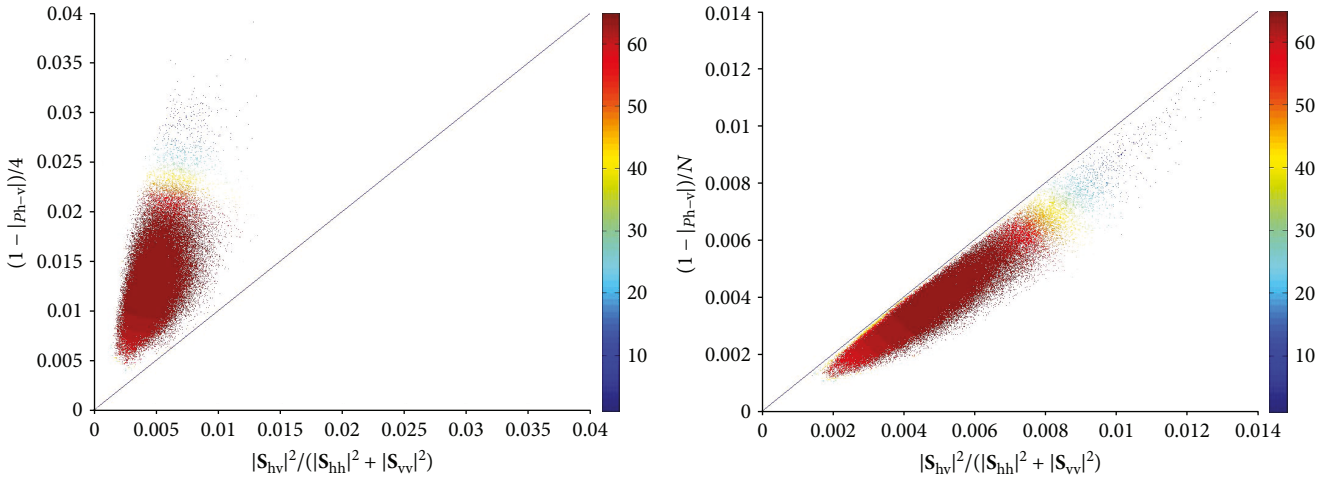

(a) Souyris' algorithm (b) Nord's algorithm

FIGURE 2: Scatter plot between $|\mathbf{S}_{hv}|^2/(|\mathbf{S}_{hh}|^2 + |\mathbf{S}_{vv}|^2)$ and $(1 - \rho_{h-v})/N$. The value of N in (a) is 4 whereas in (b) it is calculated as $|\mathbf{S}_{hh} - \mathbf{S}_{vv}|^2/|\mathbf{S}_{hv}|^2$. The convergence capability is clearly illustrated.

where ξ is the ocean surface height, k is the wavenumber, $\mathbf{r}$ is the wave space vector, ω is the wave angular frequency, and cc is the complex conjugate of the series. T^{R}_{PPK} is the modulation transfer function for SAR, which includes the tilt modulation, hydrodynamic modulation, polarization angle modulation, range and azimuthal direction modulation, and velocity bunching modulation. In all modulation functions, only the tilt and polarization orientation angle modulation depend on the radar polarization [16]. Moreover, the wave slope induced by the polarization orientation angle modulation can be neglected for horizontal or vertical polarization [16]. By (18), the terms that are not sensitive to the polarization vanish and the equation can be simplified to [16]

$$\frac{\Delta\sigma_{vv}}{\sigma_{vv}} - \frac{\Delta\sigma_{hh}}{\sigma_{hh}} = \sum_k \left(T^t_{vv} - T^t_{hh}\right)\xi_k \exp\left[i(k\cdot\mathbf{r} - \omega t)\right] + c_1,$$
$$\frac{\Delta\sigma_{\varphi\varphi}}{\sigma_{\varphi\varphi}} - \frac{\Delta\sigma_{vv}}{\sigma_{vv}} = \sum_k \left(T^t_{\varphi\varphi} - T^t_{vv} + T^p_{\varphi\varphi}\right)\xi_k \exp\left[i(k\cdot\mathbf{r} - \omega t)\right] + c_2, \tag{18}$$

where c_1 and c_2 are the complex conjugates of series, respectively; T^t_{vv} and T^t_{hh} are given by [16]

$$T^t_{vv} = ik_x \frac{4 - 0.5\left(1 - \sin^2\theta\right)}{\tan\theta\left(1 - \sin^2\theta\right)}, \tag{19}$$

$$T^t_{hh} = ik_x \frac{4 - 0.5\left(1 + \sin^2\theta\right)}{\tan\theta\left(1 + \sin^2\theta\right)}, \tag{20}$$

where k_x is the radar incidence wavenumber and θ is the incidence angle. $T^t_{\varphi\varphi}$ and $T^p_{\varphi\varphi}$ are given by (16) in [16]. By consolidating the equations, the straightforward algebraic calculation can be summarized as [16]

$$\frac{\Delta\sigma_{vv}}{\sigma_{vv}} - \frac{\Delta\sigma_{hh}}{\sigma_{hh}} = -\frac{8\tan\theta}{1 + \sin^2\theta}\frac{\delta\xi}{\delta x},$$
$$\frac{\Delta\sigma_{\varphi\varphi}}{\sigma_{\varphi\varphi}} - \frac{\Delta\sigma_{vv}}{\sigma_{vv}} = A\frac{\delta\xi}{\delta x} + B\frac{\delta\xi}{\delta y}, \tag{21}$$

where $\delta\xi/\delta x$ and $\delta\xi/\delta y$ are the range and azimuthal wave slope, respectively. Parameters A and B are also given by (8) [16]. With an appropriate choice of φ, the range wave slope and azimuthal wave slope can be directly obtained. The wave slope spectrum and the other wave parameters can be estimated from wave slope.

4. Results and Discussion

4.1. Comparision of Reconstruction Algorithms. Besides the reflectional symmetry hypothesis, the relation between the copolarized and cross-polarized responses is the main condition limiting the solution of the CP reconstruction equations [21, 34].

$$\frac{|\mathbf{S}_{hv}|^2}{|\mathbf{S}_{hh}|^2 + |\mathbf{S}_{vv}|^2} \approx \frac{1 - \rho_{h-v}}{N}. \tag{22}$$

Although both Souyris et al.'s [21] and Nord et al.'s [34] algorithms are used to reconstruct pseudo quad-polarized data, they differ in their definitions of N. Souyris et al. use 4 as the value of N, while Nord et al. calculate the value as

$$N = \frac{|\mathbf{S}_{hh} - \mathbf{S}_{vv}|^2}{|\mathbf{S}_{hv}|^2}. \tag{23}$$

We, therefore, used the two reconstruction algorithms to calculate the slope rate of curve between $|\mathbf{S}_{hv}|^2/|\mathbf{S}_{hh}|^2 + \mathbf{S}_{vv}{}^2$ and $(1 - \rho_{h-v}/N)$ (Figure 2). It is important to note that N in Figure 2(a) is equal to 4 while in Figure 2(b)N is given

Table 3: Convergence capability for CP reconstruction as found using Souyris' and Nord's algorithms.

Image ID	Total number of pixels	Number of nonconvergent pixels			
		CTLR_Souyris	$\pi/4$_Souyris	CTLR_Nord	$\pi/4$_Nord
1	6,220,800	7651	11,341	3962	1612
2	4,176,000	173	344	41	81

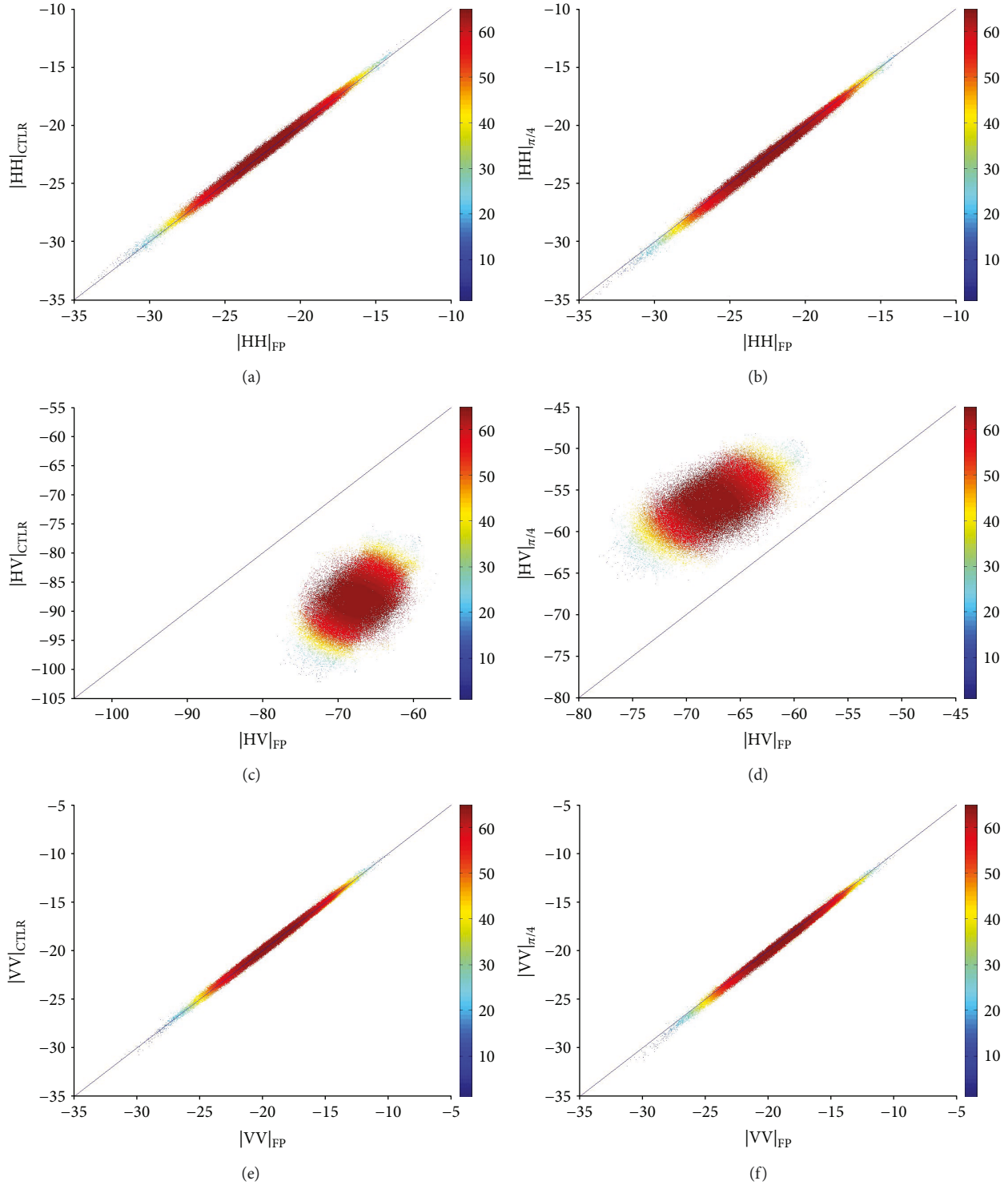

Figure 3: Reconstruction performance for HH, HV, and VV channels: scatter plots of FP and CP. (a), (c), and (e) correspond to the CTLR mode; (b), (d), and (f) correspond to the $\pi/4$ mode.

Table 4: Reconstruction accuracy of different polarized parameters for CTLR and $\pi/4$ modes.

Mode	σ_{hh}	σ_{hv}	σ_{vv}	ρ	l_1	l_2	l_3
CTLR	−0.0118	0.8658	−0.0050	0.0184	0.0014	−0.3394	0.8521
$\pi/4$	0.0205	−2.0466	0.0183	0.0202	0.0289	−0.3300	−0.3577

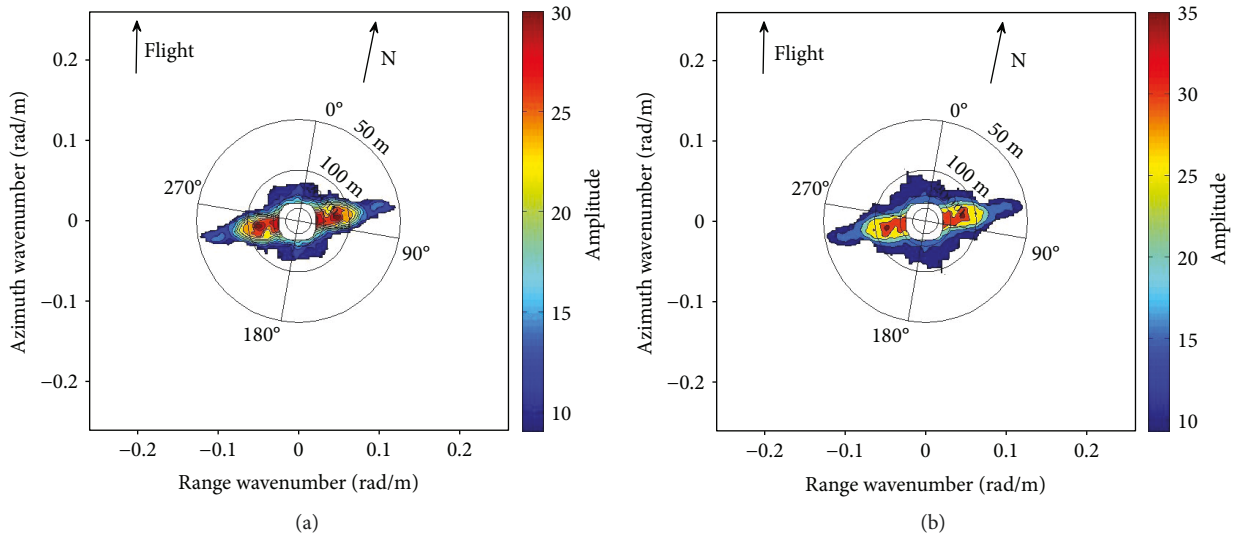

Figure 4: Ocean wave slope spectra derived from (a) FP data and (b) CP (CTLR mode) data (b). The color bar represents the wave energy amplitude.

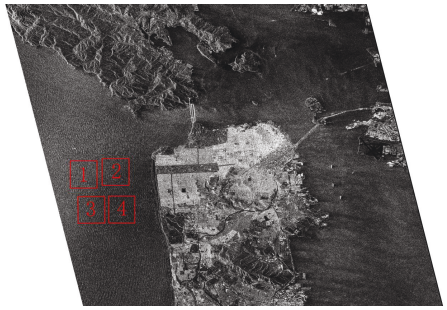

Figure 5: The positions of subimages used for ocean information retrieval in scene 2, 1–4 represent four 512×512 pixel size subimage.

by $|\mathbf{S}_{hh} - \mathbf{S}_{vv}|^2/|\mathbf{S}_{hv}|^2$, the value of which was calculated from FP data. We found that the convergence of Figure 2(a) was much inferior to Figure 2(b); the correlation coefficients, r, were equal to 0.53 and 0.93, respectively. To determine the optimum algorithm, we also calculated statistics for the nonconvergence of pixels during the reconstruction process. The results for this are shown in Table 3. The number of nonconvergent pixels found when using the two subimages of the ocean surface was much lower for Nord's algorithm than for Souyris' algorithm. Nord's algorithm is, therefore, more suitable for reconstructing pseudo quad-polarized data of the ocean surface.

4.2. Evaluation of CP Reconstruction Accuracy. CP SAR has three main modes: CTLR mode, DCP mode, and $\pi/4$ mode. Each CP mode has different orientation and ellipticity angles, which describe the transmitted and received wave status. Because of the linear relationship between the DCP and CTLR modes, these two modes have similar polarization information; therefore, we discuss only the $\pi/4$ mode and the CTLR mode in this paper. Figure 3 shows scatter plots detailing how well the derived pseudo quad-pol results fit the original quad-pol ones. The figure shows that the values of σ_{hh} and σ_{vv} between FP and CP are concentrated along the one-to-one line, which means that for σ_{hh} and σ_{vv}, the reconstruction of the pseudo quad-polarized data was good. However, the reconstruction of σ_{hv} shows a slight underestimation in the CTLR mode and an overestimation in the $\pi/4$ mode, which means that the reconstruction of σ_{hv} was not as good as for σ_{hh} and σ_{vv}. The reason for the low reconstruction accuracy for σ_{hv} may be related to the weak volume scattering at the ocean surface. It has been previously documented that the CP reconstruction algorithms are generally applied to fields and forests, where the total scattering contains a strong volume scattering component. However, the cross-polarization information is not directly used in our paper, Therefore, the inferior reconstruction performance of σ_{hv} will not make any influence on retrieval results.

To examine the reconstruction performance in more detail, we also selected 7 types of polarization parameters, including copolarization backscattering coefficientσ_{hh}, σ_{vv}, cross-polarization backscattering coefficientσ_{hv}, copolarization correlation coefficientρ, and coherence matrix eigenvaluesl_1, l_2, andl_3, for each parameter, calculating the reconstruction accuracy for the CTLR and $\pi/4$ modes. The

Table 5: Comparison of ocean parameters derived from FP quad-pol and CP CTLR mode pseudo quad-pol data with NDBC buoy measurements.

Parameters	Mode	Zone	Retrieved value	Buoy	Error	Average error
Dominant wave height (m)	Fp	1	1.99	2.18	0.19	0.14
		2	2.35		0.17	
		3	2.34		0.16	
		4	2.14		0.04	
	Cp	1	2.37		0.19	0.36
		2	2.69		0.51	
		3	2.62		0.44	
		4	2.38		0.20	
Wave direction (°)	Fp	1	259.1	246	19.25	17.12
		2	264.57		19.38	
		3	265.06		18.02	
		4	263.73		15.19	
	Cp	1	265.25		13.1	17.96
		2	265.38		18.57	
		3	264.02		19.06	
		4	261.19		17.73	
Wave period (s)	Fp	1	14.41	14.29	0.12	0.61
		2	13.74		0.54	
		3	12.72		1.56	
		4	14.52		0.23	
	Cp	1	14.01		0.27	0.88
		2	13.31		0.97	
		3	12.58		1.70	
		4	14.88		0.59	

reconstruction accuracy $(\mathrm{Pol}_{\mathrm{cp}} - \mathrm{Pol}_{\mathrm{fp}})/\mathrm{Pol}_{\mathrm{fp}}$ was used to describe the amount of deviation in the CP reconstruction. The reconstruction accuracies for σ_{hh}, σ_{hv}, σ_{vv}, ρ, l_1, l_2, and l_3 are listed in Table 4. We used the descriptions "high," "medium," and "low" to describe the deviations, where "high" was defined as less than 10%, "medium" corresponded to 10%–30%, and "low" was defined as larger than 30%. Table 4 shows that, for both the CTLR and $\pi/4$ modes, the reconstruction accuracy for the parameters σ_{hh}, σ_{vv}, ρ, and l_1 was high, with the values for the CTLR mode being superior to those for the $\pi/4$ mode. We, therefore, decided to use the CRTL mode for the subsequent ocean surface parameter reconstruction and ocean wave slope spectrum retrieval.

4.3. Retrieval of Ocean Wave Slope Spectra. In this section, we describe how Nord's algorithm was used to reconstruct the pseudo quad-pol data in the CTLR mode. The retrieved ocean wave slope spectra based on the reconstructed pseudo quad-polarized data are shown in Figure 4. Compared with the ocean wave slope spectrum derived from the FP data, the results for the CP CTLR mode obtained in this study are satisfied. It is also clear that the wave slope spectrum derived from FP presents more details compared to that derived from the CP data. However, the two wave slope spectra are similar on the whole.

In order to make a quantitative assessment of the wave retrieval results, the main wave parameters of dominant wave height, wave direction, and wave period were also extracted from the wave slope spectra and compared with the NDBC buoy data. The expressions of main wave parameters are

$$\begin{aligned} H_{\mathrm{d}} &= \tan\left(S_{\mathrm{rms}}\right)\frac{\lambda_{\mathrm{d}}}{2}, \\ \mathrm{WD}_{\mathrm{d}} &= \tan\left(\frac{\lambda_{\mathrm{d\_az}}}{\lambda_{\mathrm{d\_r}}}\right), \\ \mathrm{WP}_{\mathrm{d}} &= \frac{2\pi}{\sqrt{k_{\mathrm{d}} g \tan h(k_{\mathrm{d}} h)}}, \end{aligned} \tag{24}$$

where S_{rms} represents the root mean square of wave slope, λ_{d} represents the dominated wave length, $\lambda_{\mathrm{d\_az}}$ and $\lambda_{\mathrm{d\_r}}$, respectively, represent the components of λ_{d} in azimuth and range direction, k_{d} is the dominated wavenumber, g is acceleration of gravity, and h is the water depth.

Figure 5 shows four subimages' position which is performed to retrieve result statistics, and the 180° ambiguity of wave slope spectrum has been removed according to the measured wind direction of buoy. The results shown in Table 5 show that the average errors in the dominant wave height, wave direction, and wave period derived from the FP data are 0.14, 17.12, and 0.61, while those derived from

the CP data are 0.36, 17.96, and 0.88, respectively. It should be noted that, although the average errors in the dominant wave height, wave direction, and wave period derived from the FP data were much larger than for the CP, the retrieved CP SAR results are also satisfactory for ocean wave measurements. It is also true that the retrieval accuracy obtained using CP SAR in this study was limited by the reconstruction of the CP pseudo quad-pol data—this was especially due to the loss in precision for σ_{hv}. In future studies, the retrieval accuracy obtained using CP SAR will need to be improved.

5. Conclusion

In this paper, we investigated the capacity and potential of CP for ocean wave measurement. A Radarsat-2 quad-polarized image was used to reconstruct CP pseudo quad-polarized data and validate the potential of this for ocean slope spectrum retrieval. The main conclusions of this study are as follows.

For ocean surface waves, Nord's reconstruction algorithm is much more effective than Souyris'. Because of its convergence capacity and iteration time, we recommend adopting Nord's algorithm for the reconstruction of CP pseudo quad-polarized data.

For both the CTLR and $\pi/4$ modes, the reconstruction accuracy for the parameters σ_{hh}, σ_{vv}, ρ, and l_1 was high whereas for σ_{hv}, l_2, and l_3 it was low. In terms of the retrieval of ocean wave slope spectra using the CP mode, the CTLR mode is superior to the $\pi/4$ mode and, therefore, for the retrieval of ocean wave slope spectra, we recommend using the CTLR mode.

The potential of CP for ocean wave slope spectrum retrieval has been demonstrated in this paper. The values for the main wave parameters were also validated using in situ NDBC buoy data. A comparison of the CP SAR-based wave field information with the buoy outputs showed good agreement in terms of the dominant wave height, wave direction, and wave period, with biases of 0.36 m, 17.96°, and 0.88 s, respectively. Overall, the results for the retrieval of ocean wave slope spectra and ocean wave parameters using CP SAR were satisfactory. Moreover, considering only single SAR imagery is performed to wave retrieval algorithm study, the universality validation of ocean wave information retrieval from CP SAR will still need more results to support. In our future study, we will collect more quad-pol SAR to match up with buoy for plotting the wave parameter difference between FP and CP SAR precisely.

Conflicts of Interest

The authors declare that they have no conflicts of interest regarding the publication of this article.

Acknowledgments

The authors gratefully acknowledge the financial support provided by the National Key Research and Development Program of China (2016YFB0502504, 2016YFB0502500) and National Science Foundation of China under Grant nos. 41301500, 41431174, 61471358, and 41401427. This article is partly sponsored by the scholarship funding from the Chinese Academy of Sciences. The authors would also like to acknowledge Professor Zhang from the First Institute of Oceanography, State Oceanic Administration, for supporting research on CP theory. The authors would also like to acknowledge Dr. Bian and Dr. Liu from Institute of Remote Sensing and Digital Earth for polishing the original manuscript.

References

[1] J. Chen, Z. Lee, C. Hu, and J. Wei, "Improving satellite data products for open oceans with a scheme to correct the residual errors in remote sensing reflectance," *Journal of Geophysical Research Oceans*, vol. 121, no. 6, pp. 3866–3886, 2016.

[2] J. Chen, X. He, B. Zhou, and D. Pan, "Deriving colored dissolved organic matter absorption coefficient from ocean color with a neural quasi-analytical algorithm," *Journal of Geophysical Research Oceans*, vol. 122, no. 11, pp. 8543–8556, 2017.

[3] S. K. Chaturvedi, P. Shanmugam, C. S. Yang, and U. Guven, "Detection of ocean wave parameters using synthetic aperture radar (SAR) data," *Journal of Navigation*, vol. 66, no. 2, pp. 283–293, 2013.

[4] D. Kim, "Wind retrieval from X-band SAR image using numerical ocean scattering model," *Korean Journal of Remote Sensing*, vol. 25, no. 3, pp. 243–253, 2009.

[5] M. Sugimoto, N. Shiroto, and K. Ouchi, "Estimation of ocean wave height using polarization ratio of synthetic aperture radar data," in *2011 IEEE International Geoscience and Remote Sensing Symposium (IGARSS)*, pp. 2821–2824, Vancouver, BC, Canada, July 2011.

[6] P. W. Vachon, H. E. Krogstad, and J. S. Paterson, "Airborne and spaceborne synthetic aperture radar observations of ocean waves," *Atmosphere-Ocean*, vol. 32, no. 1, pp. 83–112, 1994.

[7] K. Hasselmann and S. Hasselmann, "On the nonlinear mapping of an ocean wave spectrum into a synthetic aperture radar image spectrum and its inversion," *Journal of Geophysical Research Oceans*, vol. 96, no. C6, pp. 10713–10729, 1991.

[8] S. Hasselmann and K. Hasselmann, "Computations and parameterizations of the nonlinear energy transfer in a gravity-wave spectrum. Part I: a new method for efficient computations of the exact nonlinear transfer integral," *Journal of Physical Oceanography*, vol. 15, no. 11, pp. 1369–1377, 1985.

[9] C. Mastenbroek and C. F. de Valk, "A semiparametric algorithm to retrieve ocean wave spectra from synthetic aperture radar," *Journal of Geophysical Research Oceans*, vol. 105, no. C2, pp. 3497–3516, 2000.

[10] H. Wang, J. Zhu, J. Yang, and C. Shi, "A semiempirical algorithm for SAR wave height retrieval and its validation using Envisat ASAR wave mode data," *Acta Oceanologica Sinica*, vol. 31, no. 3, pp. 59–66, 2012.

[11] W. Shao, Z. Zhang, X. Li, and H. Li, "Ocean wave parameters retrieval from Sentinel-1 SAR imagery," *Remote Sensing*, vol. 8, no. 9, 2016.

[12] B. Zhang, X. Li, W. Perrie, and Y. He, "Synergistic measurements of ocean winds and waves from SAR," *Journal of Geophysical Research Oceans*, vol. 120, no. 9, pp. 6164–6184, 2015.

[13] D. L. SCHULER and J. S. LEE, "A microwave technique to improve the measurement of directional ocean wave spectra,"

International Journal of Remote Sensing, vol. 16, no. 2, pp. 199–215, 1995.

[14] D. L. Schuler, J. S. Lee, D. Kasilingam, and E. Pottier, "Measurement of ocean surface slopes and wave spectra using polarimetric SAR image data," *Remote Sensing of Environment*, vol. 91, no. 2, pp. 198–211, 2004.

[15] Y. He, H. Shen, and W. Perrie, "Remote sensing of ocean waves by polarimetric SAR," *Journal of Atmospheric and Oceanic Technology*, vol. 23, no. 12, pp. 1768–1773, 2006.

[16] Y. He, W. Perrie, T. Xie, and Q. Zou, "Ocean wave spectra from a linear polarimetric SAR," *IEEE Transactions on Geoscience and Remote Sensing*, vol. 42, no. 11, pp. 2623–2631, 2004.

[17] B. Zhang, W. Perrie, and Y. He, "Validation of RADARSAT-2 fully polarimetric SAR measurements of ocean surface waves," *Journal of Geophysical Research Oceans*, vol. 115, no. C6, pp. 302–315, 2010.

[18] Y. He, B. Zhang, and W. Perrie, "Validation of RADARSAT-2 polarimetric SAR measurements of ocean waves," in *2009 IEEE International Geoscience and Remote Sensing Symposium*, pp. III-168–III-171, Cape Town, South Africa, July 2009.

[19] R. L. Paes, F. Nunziata, and M. Migliaccio, "On the capability of hybrid-polarity features to observe metallic targets at sea," *IEEE Journal of Oceanic Engineering*, vol. 41, no. 2, pp. 346–361, 2016.

[20] R. K. Raney, "A perspective on compact polarimetry," *IEEE Geoscience and Remote Sensing Letters*, vol. 160, pp. 12–18, 2011.

[21] J.-C. Souyris, P. Imbo, R. Fjortoft, S. Mingot, and J.-S. Lee, "Compact polarimetry based on symmetry properties of geophysical media: the $\pi/4$ mode," *IEEE Transactions on Geoscience and Remote Sensing*, vol. 43, no. 3, pp. 634–646, 2005.

[22] F. Nunziata, M. Migliaccio, and X. Li, "Sea oil slick observation using hybrid-polarity SAR architecture," *IEEE Journal of Oceanic Engineering*, vol. 40, no. 2, pp. 426–440, 2015.

[23] J. Yin, J. Yang, Z. S. Zhou, and J. Song, "The extended Bragg scattering model-based method for ship and oil-spill observation using compact polarimetric SAR," *IEEE Journal of Selected Topics in Applied Earth Observations and Remote Sensing*, vol. 8, no. 8, pp. 3760–3772, 2015.

[24] T. Geldsetzer, F. Charbonneau, M. Arkett, and T. Zagon, "Ocean wind study using simulated RCM compact-polarimetry SAR," *Canadian Journal of Remote Sensing*, vol. 41, no. 5, pp. 418–430, 2015.

[25] H. Li, J. Wu, W. Perrie, and Y. He, "Wind speed retrieval from hybrid-pol compact polarization synthetic aperture radar images," *IEEE Journal of Oceanic Engineering*, no. 99, pp. 1–12, 2017.

[26] R. Shirvany, M. Chabert, and J. Y. Tourneret, "Ship and oil-spill detection using the degree of polarization in linear and hybrid/compact dual-pol SAR," *IEEE Journal of Selected Topics in Applied Earth Observations and Remote Sensing*, vol. 5, no. 3, pp. 885–892, 2012.

[27] R. Touzi and F. Charbonneau, "Requirements on the calibration of hybrid-compact SAR," in *2014 IEEE Geoscience and Remote Sensing Symposium*, pp. 1109–1112, Quebec City, QC, Canada, July 2014.

[28] S. Boularbah, M. Ouarzeddine, and A. Belhadj-Aissa, "Investigation of the capability of the compact polarimetry mode to reconstruct full polarimetry mode using RADARSAT2 data," *Advanced Electromagnetics*, vol. 1, no. 1, p. 19, 2012.

[29] X. Zhang, J. Zhang, M. Liu, and J. Meng, "Assessment of C-band compact polarimetry SAR for sea ice classification," *Acta Oceanologica Sinica*, vol. 35, no. 5, pp. 79–88, 2016.

[30] P. C. Dubois-Fernandez, J. C. Souyris, S. Angelliaume, and F. Garestier, "The compact polarimetry alternative for spaceborne SAR at low frequency," *IEEE Transactions on Geoscience and Remote Sensing*, vol. 46, no. 10, pp. 3208–3222, 2008.

[31] J. J. van Zyl, H. A. Zebker, and C. Elachi, "Imaging radar polarization signatures: theory and observation," *Radio Science*, vol. 22, no. 4, pp. 529–543, 1987.

[32] J.-S. Lee, D. L. Schuler, and T. L. Ainsworth, "Polarimetric SAR data compensation for terrain azimuth slope variation," *IEEE Transactions on Geoscience and Remote Sensing*, vol. 38, no. 5, pp. 2153–2163, 2000.

[33] J.-S. Lee, D. L. Schuler, T. L. Ainsworth, E. Krogager, D. Kasilingam, and W.-M. Boerner, "On the estimation of radar polarization orientation shifts induced by terrain slopes," *IEEE Transactions on Geoscience and Remote Sensing*, vol. 40, no. 1, pp. 30–41, 2002.

[34] M. E. Nord, T. L. Ainsworth, J. S. Lee, and N. J. S. Stacy, "Comparison of compact polarimetric synthetic aperture radar modes," *IEEE Transactions on Geoscience and Remote Sensing*, vol. 47, no. 1, pp. 174–188, 2009.